ACS APPLIED ELECTRONIC MATERIALS

UNM

Subscriber access provided by The University of New Mexico

Article

Revealing Temperature Dependent Absorption and Emission Enhancement Factors in Plasmon Coupled Semiconductor Heterostructures

Chih-Feng Wang, Sadhvikas Addamane, Bisweswar Patra, Claudia Rivera Lebron, Sharmin Haq, Ganesh Balakrishnan, Kevin J. Malloy, and Terefe G. Habteyes

ACS Appl. Electron. Mater., **Just Accepted Manuscript** • DOI: 10.1021/acsaelm.9b00252 • Publication Date (Web): 08 Jul 2019

Revealing Temperature Dependent Absorption and Emission Enhancement Factors in Plasmon Coupled Semiconductor Heterostructures

Chih-Feng Wang,[†] Sadhvikas Addamane,[†] Bisweswar Patra,[†] Claudia Rivera Lebron,[†] Sharmin Haq,[†] Ganesh Balakrishnan,[†,‡] Kevin J. Malloy,[†] and Terefe G. Habteyes*[,†,§]

[†]*Center for High Technology Materials, Departments of* [§]*Chemistry and Chemical Biology, and* [‡]*Electrical & Computer Engineering, University of New Mexico, Albuquerque, New Mexico 87131, United States*

KEYWORDS: Plasmon-enhanced absorption, spontaneous emission, Purcell factor, external quantum efficiency, photoluminescence, carrier diffusion, InGaAs/GaAs quantum well, gold nanorods

Abstract. Localized surface plasmon resonances can increase the quantum efficiency of photon emitters through both absorption and spontaneous emission enhancement effects. Despite extensive studies, experimental results that clearly distinguish the two plasmonic enhancement effects are rarely available. Here, we present clear spectral signatures of the plasmonic enhancement effects on the absorption (excitation) and spontaneous emission (Purcell factor) by analyzing the temperature dependent photoluminescence (PL) properties of InGaAs/GaAs single quantum well (QW) coupled to colloidal gold nanorods (AuNRs) at different GaAs capping layer

thickness (d). We find that when the emitting InGaAs layer is close to the AuNRs (d = 5 nm), the plasmonic enhancement effect on the QW PL is dominated by the Purcell factor that significantly increases the external quantum efficiency of the QW that otherwise barely emits. When d is increased to 10 nm, the temperature dependence of the PL enhancement factor (F) reflects absorption enhancement in the capping layer followed by carrier diffusion and capture by the well. First F increases with temperature and then decreases following the temperature dependence of the carrier diffusion coefficient in GaAs. By factoring out the contribution of the captured carriers to F, it is shown that carrier transfer to the well reaches saturation with increasing incident laser power. In addition to providing insight into the plasmonic enhancement mechanism, the results presented in this work suggest that colloidal plasmonic nanoparticles can be used as simple probes for understanding carrier transport phenomena in arbitrary semiconductor heterostructures.

1. INTRODUCTION

Understanding the fundamental photophysical processes at the interfaces of coupled plamonic and excitonic systems is essential in conceptualizing and designing plasmonic hybrid devices for a variety of applications including photon emission,[1-13] photodetection,[14-19] lasing,[20-22] photovoltaics,[23-25] photocatalysis,[26-30] photon upconversion,[31] and energy transfer.[32] When optically active molecules and semiconductors are photoexcited in the proximity of plasmonic metal nanoparticles, their photon absorption and emission efficiencies can be enhanced significantly by the high density of localized surface plasmon field provided that the plasmon resonances spectrally overlap with the excitation and emission frequencies of the active materials.[33, 34] The contribution of the absorption and spontaneous emission enhancements to the

external quantum efficiency of an emitter have been theoretically described by Khurgin and co-workers.[35, 36] It is, however, difficult to experimentally quantify the contribution of absorption and emission enhancements as both effects can result in the overall increase of the measured intensity.[37, 38] That is, the total PL intensity enhancement factor (F) is determined by the product of absorption enhancement factor (F_a) and emission enhancement factor (F_e) as $F = F_aF_e$, where F_e is determined from the Purcell factor (F_P) using the following relation.[36]

$$F_e = \frac{1 + F_P\eta_{pr}}{1 + F_P\eta_r} \quad (1)$$

where η_r is the radiative efficiency of the emitter without the plasmonic enhancement effect, which is determined by the rate constants of the radiative (k_r) and nonradiative (k_{nr}) excited state decay processes as $\eta_r = k_r/(k_r + k_{nr})$, and η_{pr} is the efficiency of converting internal modes to photons through the surface plasmon modes.

In this work, the contributions of absorption and spontaneous emission enhancements to the measured PL intensity are investigated as a function of temperature using InGaAs/GaAs single QW coupled to colloidal AuNRs as model system. The sample is excited using 1.96 eV photon energy, which is above the bandgap energy of GaAs (<1.52 eV depending on temperature[39, 40]). It is important to note that plasmon enhanced absorption is limited by the near-field decay length into the GaAs capping layer, and becomes insignificant deeper than 10 nm at 633 nm excitation wavelength.[41] In general, in plasmonic coupling to semiconductors, the excitation action is confined at the metal-semiconductor interface.[42] As a result, the QW PL enhancement due to plasmon enhanced excitation involves diffusion and transfer of carriers from the GaAs capping layer to the InGaAs well. At the emission wavelength (λ ~920 nm), GaAs is transparent and the QW-plasmon coupling length can be longer. The discussion in this work includes consideration

of absorption enhancement, carrier diffusion/capture and plasmon enhanced spontaneous emission.

Our analysis reveal the dominance of the Purcell factor or absorption enhancement effects depending on the thickness (d) of the GaAs capping layer that serves as active medium at the excitation wavelength and transparent spacer at the emission wavelength. For d = 5 nm, the plasmonic enhancement effect on the QW PL is dominated by the Purcell factor that improves the radiation efficiency of otherwise dark states as evidenced in about 30 fold intensity enhancement accompanied by drastic spectral narrowing. For d = 10 nm, the PL enhancement factor has an interesting temperature dependence that can be described by a Gaussian function, and up to 80 fold intensity enhancement is observed at the peak temperature. For d = 10 nm, the intensity enhancement is accompanied by spectral broadening, indicating the dominance of absorption enhancement and free carrier diffusion from the barrier to the well. The temperature dependence of the PL enhancement factor parallels that of the carrier diffusion coefficient in GaAs. We note that in addition to providing insight into the enhancement mechanism, the experimental approach described in this work can be extended to determine carrier diffusion lengths and lifetimes in semiconductor heterostructures.

2. METHODS

2.1 Coupling geometry and sample fabrication. The coupling geometry of a gold nanorods and InGaAs/GaAs single QW is shown in the schematic in Figure 1a. QWs with GaAs capping layer thicknesses of 5, 10 and 15 nm are grown in a VG V80 molecular beam epitaxy (MBE) reactor on epi-ready semi-insulating GaAs (001) substrates. The substrate temperature is measured using an optical pyrometer and the surface is monitored using reflection high-energy electron diffraction (RHEED). Prior to growth, the native oxide on the substrates is thermally

desorbed at 630 °C for 20 minutes under a constant AS3 overpressure. The substrate temperature is then brought down to 580 °C and a 150 nm thick GaAs smoothing layer is grown. At this point, a 2×4 reconstruction is observed on the RHEED pattern, indicating a smooth GaAs surface. Next, the temperature is further decreased to 475 °C for the growth of the active medium. The active medium consists of an 8.35 nm thick $In_{0.18}Ga_{0.82}As$ layer capped with 1.55 nm GaAs layer. The thin GaAs cap is included to protect the QW during the subsequent temperature transition. Following the growth of the active medium, the substrate temperature is increased back up to 580 °C to grow a high-temperature GaAs cap. Three different samples are grown with varying thicknesses of the high-temperature GaAs cap so that the total cap (thin cold GaAs + high-temperature cap) thickness adds up to 5, 10 and 15 nm. In all cases, the In and Ga growth rates (calibrated by RHEED oscillations) were kept constant at 0.065 and 0.3 ML/sec and a constant As:Ga beam equivalent pressure (BEP) ratio of 13 is maintained.

Aqueous solution of gold nanorods was obtained from Nanopartz, Inc. After removing the excess surfactant through centrifugation and re-suspension procedures, the AuNRs were drop-casted on some portion of the GaAs capping layer surface that has been exposed to ambient air. The drop-casting procedure produces random distribution of AuNRs, resulting in 5 – 10 % coverage of the GaAs surface on which the solution is applied and dried.[41]

2.2 Optical measurements. The optical responses of the AuNRs on GaAs surface is characterized using dark-field scattering spectroscopy as described elsewhere.[41, 43] The temperature-dependent PL (TDPL) measurement is performed using a home-built optical setup, which is shown by the schematic in Figure 1b. The InGaAs/GaAs QW was mounted on a cryostat chamber (CTI-Cryogenics, Model 22), two stage, closed-cycle helium refrigeration system. The temperature can be varied from 10 K to room temperature at user defined intervals.

The output of a HeNe laser, $\lambda = 633$ nm, is used for exciting the sample at incidence angle of 10 degree with respect to the surface normal. The spectra are acquired using conventional lock-in technique utilizing 50 cm focal length monochromator (ARC SpectraPro-500). The excitation light is focused using 0.2 NA lens to a spot diameter of 400 μm as determined using knife edge method. The PL signal is collected using the same lens and detected by a Femtowatt Photoreceiver (New Focus, Inc., Model 2153). The TDPL measurement is automated by developing LabVIEW program in-house. The PL spectra are recorded at every 2.5 K or 5 K increment. After each increment, sufficient time (at least 5 minutes) is allowed for stabilization so that the accuracy of the temperature is within 0.2 K. The plasmonic enhancement effect is studied by comparing the PL spectra of the sample region where about 0.5 – 5% of the area (see Figures S1) is covered with the AuNRs to the spectra of the region where there are no AuNRs.

3. RESULTS AND DISCUSSION

The near-field and far-field properties of AuNRs on GaAs are illustrated in Figures 1c and 1d, respectively. The spectral line shape of the individual AuNRs on GaAs can vary depending on the size distribution[44] and sub-nanometer variation of the inherent dielectric spacing between the AuNRs and the GaAs due to the native oxide on GaAs and the surface ligand on the AuNRs. As discussed in detail in our earlier report,[41] the scattering spectra of individual AuNRs on GaAs ranges from weak scattering intensity non-Lorentzian line shapes (dotted blue line in Figure 1d) to strong intensity Lorentzian shapes (dashed blue line in Figure 1d) presumably due to the variation of the interfacial dielectric spacing. Our measurement is based on aggregates (Figure S1) of AuNRs on the GaAs capping layer. For aggregates, interparticle dipole-dipole plasmon coupling can shift the plasmon resonance energy to the red significantly depending on the proximity and orientation of the nanorods.[45-49] This distance and orientation dependent red-

shifting results in spectral broadening as shown by the solid blue line in Figure 1d, and improves the spectral overlap with both excitation and emission energies. Starting from its bandgap energy, the absorption coefficient of GaAs increases with photon energy as shown by the black line in Figure 1d, and the excitation of the plasmon resonances increases the local electric field intensity resulting in plasmon-enhanced absorption.[34, 35] Hence, the coupling of the AuNRs to the QW as shown in Figure 1a is expected to enhance carrier generation inside the GaAs capping layer close to the metal-semiconductor interface, where the plasmon field is localized.

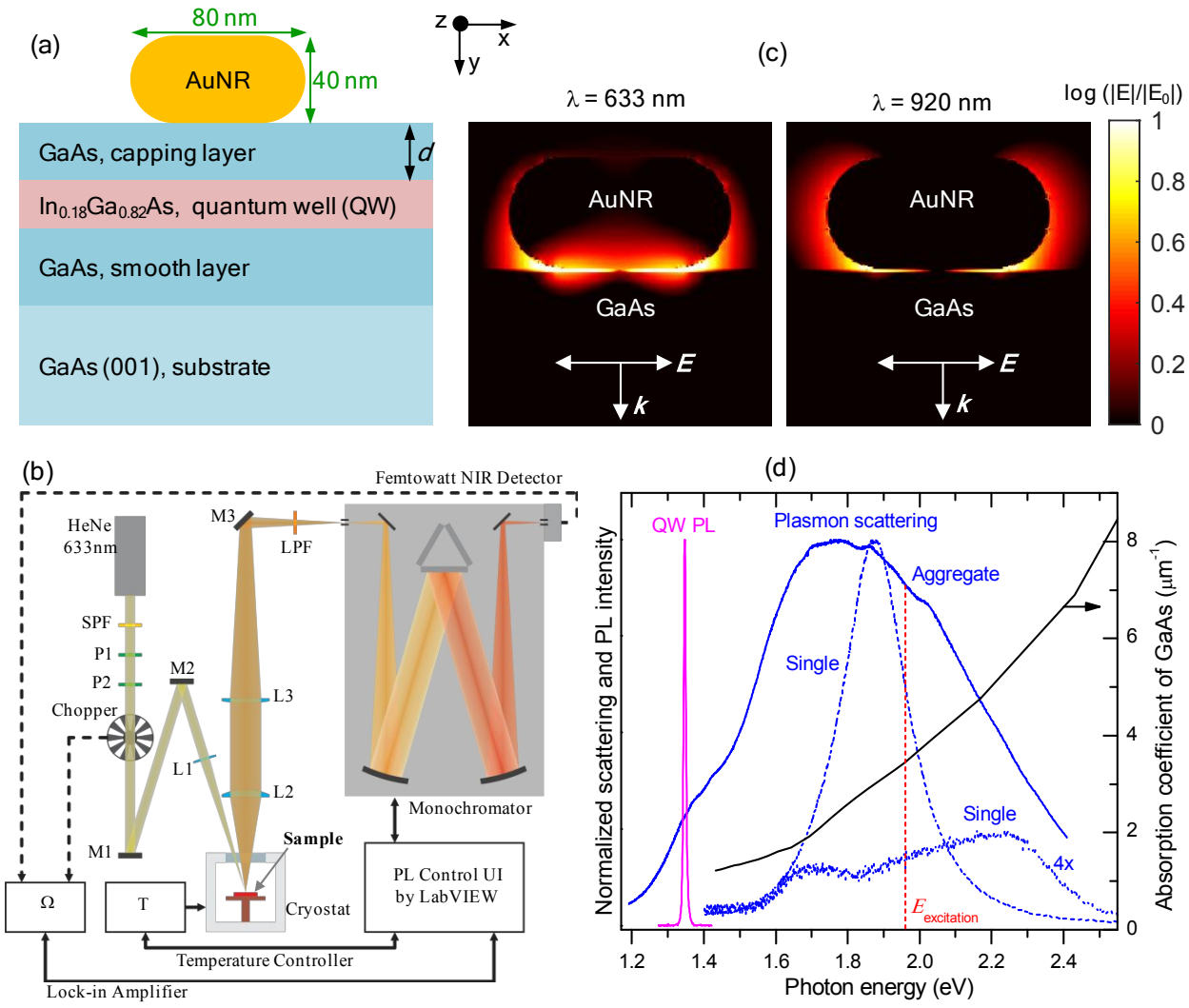

Figure 1 (a) Schematic showing the QW-AuNR coupling through the GaAs capping layer of thickness *d*. (b) Schematic of the optical layout used for the temperature dependent PL measurement. SPF ≡ shortpass filter; P1, P2 ≡ polarizers; L1, L2, L3 ≡ lens; M1, M2, M3 =

mirrors; LPF ≡ longpass filter. (c) Near-field localization and enhancement at the excitation and emission wavelengths as determined using finite-difference time-domain simulation (image size = 110 nm × 110 nm). The propagation (***k***) and electric field (***E***) vectors of the excitation source are indicated on each panel using single and double headed arrows as labeled. (d) Dark-field scattering spectra of single (dashed and dotted blue lines) and aggregated (solid blue line) of AuNRs on GaAs. The excitation energy (dashed vertical red line, 1.96 eV) overlaps with the plasmon resonances that can increase the absorption coefficient of the GaAs (black line). The plasmon resonance also has appreciable overlap with the PL spectrum of the QW.

This localized plasmon pumped excitation creates carrier concentration gradient ($\frac{dn}{dy}$) along the y-direction (see Figure 1) going from the AuNR-GaAs interface region to the InGaAs layer. The flux of carriers flowing toward the well, in which radiative recombination takes place, is proportional to the product of the concentration gradient and the carrier diffusion coefficient (*D*), which can be calculated using the Einstein relation.

$$D = \left(\frac{kT}{q}\right)\mu \qquad (2)$$

where *T* is temperature, *k* is the Boltzmann constant, *q* is the charge on electron or hole, and μ is the mobility of electron or hole.

The plasmon resonances of the AuNR aggregates also overlap with the emission energy of the QW as shown by the spectral overlap between the solid blue and purple lines in Figure 1d, although to a lesser extent compared to the overlap with the absorption band. Furthermore, the results of electromagnetic simulation (see Figure S2) indicate that the near-field amplitude around the AuNR is significant at the emission wavelength (λ ~920 nm) of the QW. As a result, the plasmonic surface field is also expected to enhance the rate of spontaneous emission (Purcell enhancement effect).[7, 20, 36, 50-52] It is interesting to note that the plasmon field localization at the AuNR-GaAs interface and at the ends of the rod is different at the excitation (633 nm) and emission (920 nm) wavelengths as shown in Figure 1c. The distinction is more apparent in the x-component of the near-field amplitude and phase as shown in Figure S3. At 633 nm, the field is

mainly localized at the AuNR-GaAs interface, whereas at 920 nm, it has a dipolar character concentrating at the ends of the rod. As a result, at 633 nm, the AuNR-GaAs interface can serve as a small nanocavity to concentrate light energy thereby enhancing absorption, while at 920 nm the AuNRs serve as efficient dipole antenna to radiate photons to the far-field, fulfilling the different requirements for absorption and emission enhancements as proposed by Sun *et al*. [36] We now investigate the dominant PL enhancement mechanism as *d* increases from 5 nm to 10 nm and 15 nm.

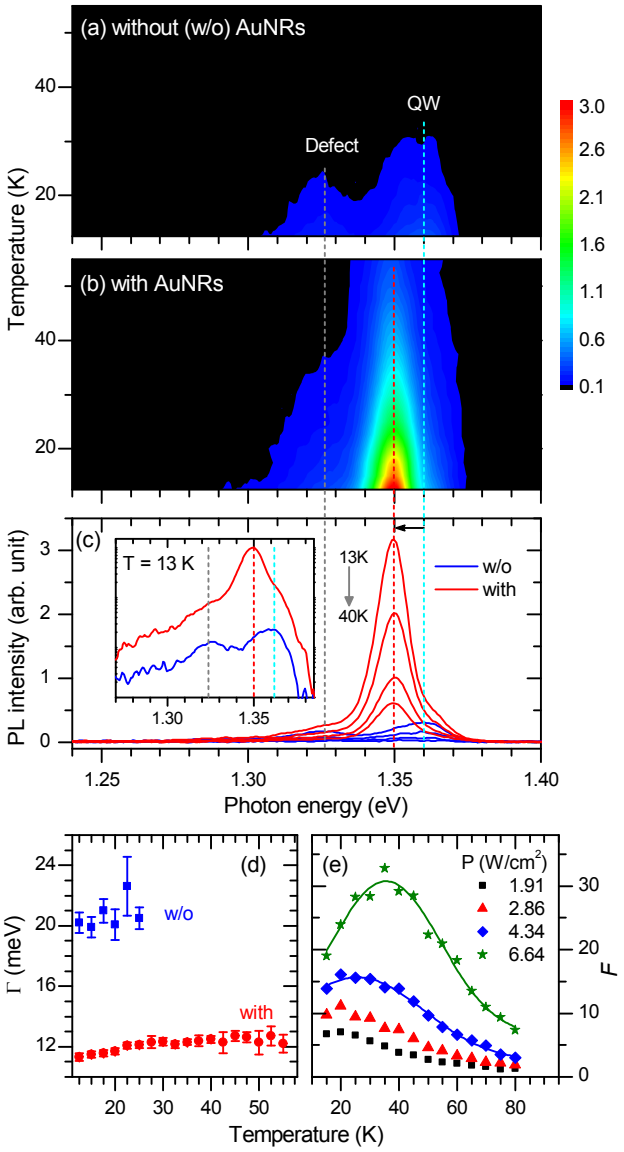

Figure 2 Plasmonic PL enhancement for the InGaAs/GaAs QW with 5 nm GaAs capping layer. (a, b) PL intensity map representing spectra recorded at every 2.5 K temperature intervals starting at 12.5 K (~13 K) in the absence (a) and presence (b) of AuNRs on the GaAs capping layer. (c) Representative PL spectra at 13, 20, 30 and 40 K with (red lines) and without (blue lines) AuNRs. The inset graph shows the spectra recorded at 13 K using log scale for the intensity. (d) Spectral linewidth (Γ = FWHM) without (blue squares) and with (red circles) AuNRs. Γ is determined by fitting Gaussian function to the data as illustrated in Figure S4. (e) PL intensity enhancement factor *F* (IPL intensity of the QW with AuNRs divided by the corresponding intensity of the bare QW) as a function of temperature at different incident laser intensity *P*. The solid lines are Gaussian fit to the data.

3.1 Brightening a defective photon emitter (*d* = 5 nm). For *d* = 5 nm, the combination of oxidized surface that is close to the emitting InGaAs layer and misfit dislocations can lead to high density of interface defects[53] [54] that become non-radiative recombination centers of photocarriers generated inside the heterostructure. As expected, the PL intensity for the QW with 5 nm GaAs cap is very weak and the spectral shape is not well defined as shown in Figure 2a even at low temperatures. In fact, the emission intensity of the broad peak at ~1.33 eV from the deep level interface defect states is comparable to the intensity of the QW PL peak at ~1.36 eV. These poor spectral characteristics are in agreement with reported results that describe degradation of structural and optical quality with decreasing capping layer thickness particularly for $d < 10$ nm.[55]

Despite this high defect density that is inherent to a single QW with shallow capping layer, our experimental observations indicate that the optical quality can be improved dramatically by coupling to colloidal AuNRs that support plasmon modes at the excitation and emission wavelengths. As can be seen by comparing the PL intensity map of the bare QW (Figures 2a) to the corresponding intensity map of the QW coupled to the AuNRs (Figure 2b) as well as the representative spectra in Figure 2c, the coupling to the plasmon modes has resulted in a significant increase of the PL intensity, which is accompanied by drastic spectral narrowing. The

spectral linewidth has decreased from 20 meV to 11 meV at 13 K, and the narrowing is maintained with increasing temperature (Figure 2d). This linewidth narrowing corresponds to an optical quality factor (peak energy to linewidth ratio) increase from ~67 to ~119 (~88% improvement). Interestingly, the plasmonic coupling has no significant effect on the intensity and position of the defect emission band. As a result, the PL spectrum is transformed essentially to a single Lorentzian peak as can be seen more clearly in the semilogarithmic plot in the inset graph in Figure 2c. In addition, the plasmonic enhancement effect has extended the range of the temperature at which emitted photons can be detected as the intensity map in Figure 2b indicate.

We note that the PL spectral pattern remain the same with increasing incident laser intensity (Figure S5), indicating that the plasmonic enhancement effect for the defective QW cannot be compensated by increasing the incident laser intensity. This observation underscores the critical importance of the plasmonic Purcell enhancement effect to increase the external quantum efficiency of the defective QW that otherwise barely emits photons. Referring to Equation 1, the brightening effect can be explained in terms of the plasmon coupled photon emission efficiency (η_{pr}) that enables conversion of internal modes to the far-field.

For further analysis, we use the PL intensity enhancement factor (F), which is defined as the ratio of the integrated PL intensity of the QW with AuNR to the intensity of the QW without the AuNRs. In Figure 2e, F obtained at different incident laser intensity (P) are plotted as a function of temperature. As mentioned in the introduction, the PL enhancement can originate from plasmon enhanced absorption, and the Purcell factor. We note that for d = 5 nm, the InGaAs layer is within the decay length of the plasmon field localized at the AuNR-GaAs interface. As a result, the plasmon field enhances excitation of the GaAs capping layer as well as the InGaAs layer directly. The initial increase of F with increasing temperature (Figure 2e) can be attributed

to free carrier diffusion and transfer from the barrier to the well.[56] Hence, when the PL enhancement is dominated by carrier capture from the barrier, the temperature dependence of F follows the temperature dependence of the carrier diffusion coefficient D. The dependence of D on temperature is mainly determined by the carrier mobility μ that, for GaAs, increases with temperature first and then decreases[57, 58] (Figure S6), which is consistent with the temperature dependence of F as shown in Figure 2e. It is also important to note that with increasing temperature, thermionic emission of carriers out of the well and non-radiative recombination processes become dominant,[59-61] which results in the decline of the enhancement factor. In addition, reported experimental and theoretical studies indicate that Purcell enhancement effect decreases with increasing temperature.[52, 62]

The data plotted in Figure 2e show that at a fixed temperature, the enhancement factor increases with increasing P. As it will be discussed later, this is an indication that the plasmonic Purcell enhancement effect that increases proportional to the plasmon field intensity[34] is the dominant PL enhancement mechanism for the QW with d = 5 nm. With increasing d, the contribution of carriers generated by plasmon pumping of the GaAs capping layer to the PL enhancement can become dominant as it will be discussed next.

3.2 Plasmon pumped barrier excitation and carrier diffusion (d = 10 nm). The plasmonic enhancement effect on the QW with capping (barrier) layer thickness d = 10 nm is presented in Figure 3. The IPL intensity plot as a function of temperature exhibits different trends in the presence and absence of the AuNRs as can be seen comparing the data shown by the blue squares and red circles in Figure 3b (see also Figure S7). In the absence of the AuNRs, a single exponential function fits the data, while it deviates from this trend in the presence of the AuNRs. In particular, with the plasmonic enhancement effect, the curve has a concave down

shape with an apparent inflection point that appears to indicate a critical temperature beyond which the contribution of the plasmon generated and captured carriers to the QW PL is declining. The enhancement factor *F*, shown by the black circles in Figure 3b, increases considerably up to the critical temperature and then decreases rapidly with temperature further increasing. By fitting a Gaussian function (solid black line in Figure 3b) to the experimentally determined enhancement factor, the average critical or peak temperature is determined as ~47 K at 0.14 W/cm^2 excitation intensity. The observed trend of *F* is in contrast to the temperature dependence of the Purcell enhancement factor reported for ZnO films[62] and InGaN/GaN QW[52] that decreases slowly with increasing temperature. Therefore, the increase in *F* up to a certain temperature for our samples can be attributed to the contribution of carriers generated by plasmon pumping of the GaAs capping layer and captured by the well. Referring to Figure S6, it can be seen that the increase in *F* with temperature parallels the temperature dependence of the carrier diffusion coefficient as mentioned in Section 3.1.

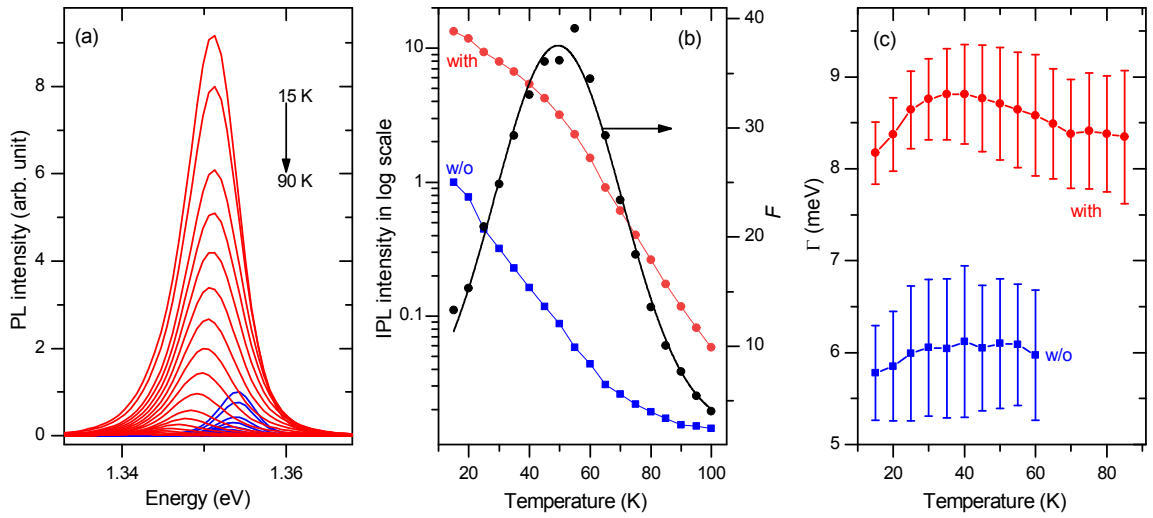

Figure 3. Temperature-dependent plasmonic enhancement effects on InGaAs/GaAs QW with *d* = 10 nm at *P* = 0.14 W/cm^2. (a) PL spectra with (red lines) and without (blue lines) AuNRs at different temperatures. (b) Left y-axis: IPL intensity as a function of temperature without (blue squares) and with (red circles) AuNRs; Right y-axis: the PL intensity enhancement factor (black

circles) as a function of temperature (the solid line is a Gaussian fit to the data). (c) The FWHM without (blue square) and with (red circles) AuNRs as a function of temperature.

As the free carriers are transferred from the GaAs barrier to the well, the linewidth is expected to increase proportional to the free carrier concentration n ($\Delta E = \frac{h^2 n}{4\pi m}$, where m is the effective mass of electron, and h is Planck's constant).[63-65] As can be seen in Figures 3c, at 15 K, Γ = 5.8 ± 0.5 meV without the AuNRs, and 8.3 ± 0.3 meV with the AuNRs, corresponding to ~41% plasmon-induced linewidth broadening, which is in contrast to the spectral narrowing observed for the QW with d = 5 nm (Figure 2d), indicating the dominance of absorption enhancement to the measured PL intensity as opposed to the dominant spontaneous emission enhancement for d = 5 nm. Similar to the trend for F, the plasmon-induced linewidth broadening appears to increase up to a certain temperature, confirming free carrier concentration increase inside the well because of enhanced rate of carrier capture from the capping layer.

Further evidence for the mechanism of the plasmonic enhancement of the QW PL can be obtained by analyzing the temperature dependence of the IPL intensity at different P as shown in Figure 4a. In the presence of the AuNRs, the deviation from a linear trend in the semilogarithmic plot is apparent even at the lowest P (0.1 W/cm^2), and the degree of the deviation increases with increasing P. Small deviation from the linear trend is also observed in the absence of the AuNRs (open symbols) when P is increased above ~2 W/cm^2, indicating that the plasmon pumped excitation can be compensated by increasing the incident laser power. However, the deviation observed at the lowest P value (solid squares) in the presence of the AuNRs is more pronounced than the deviation observed at the highest P value (open stars) in the absence of the AuNRs, which underscores the contribution of the free carriers generated by plasmon pumping of the GaAs capping layer. We note that for d = 10 nm, the material thickness including the InGaAs layer is 18 nm, which is much smaller than the penetration depth of the incident light that can be

estimated as ~250 nm from the absorption coefficient of the GaAs at λ = 633 nm (Figure 1d). As a result, generation of carriers by the incident light can be assumed uniform within the depth in which the InGaAs layer is embedded. Hence, no significant concentration gradient of carriers is expected in the absence of the AuNRs on the GaAs capping layer, making diffusion less important. Therefore, the different curvatures of the IPL intensity as a function of temperature in the presence and absence of the AuNRs as shown in Figure 4a can simply be explained in terms of the temperature dependence of the carrier diffusion coefficient.

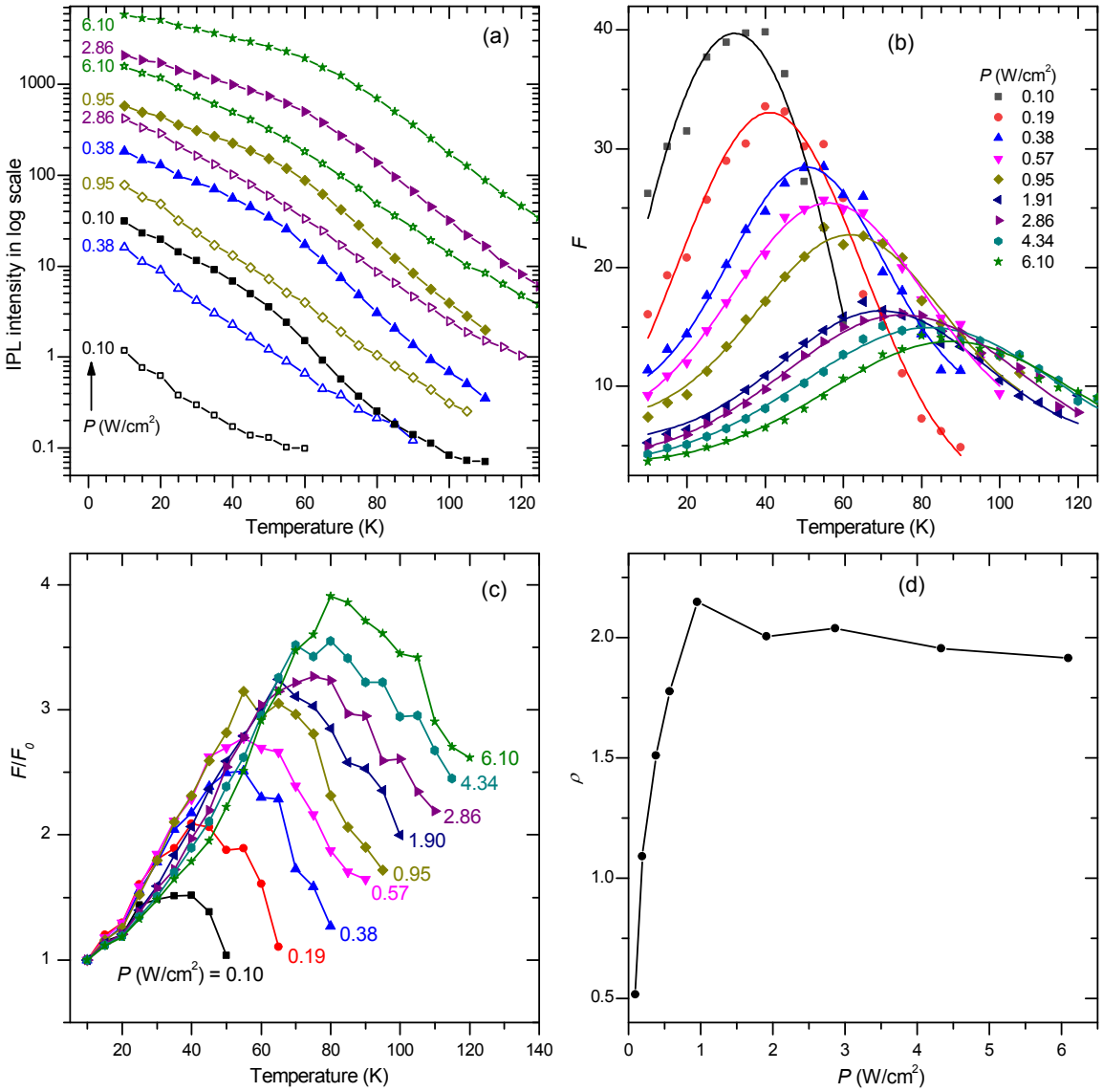

Figure 4 (a) IPL intensity (in log scale) as a function of temperature without (open symbols) and with (solid symbols) at different excitation intensities as labeled. (b) The PL intensity enhancement factor as a function of temperature at different excitation intensity. The solid lines are Gaussian fit to the data. (c) The enhancement factor normalized by the corresponding values at T = 10 K. (d) The contribution of plasmon generated and captured carriers determined using Equation (3).

At low P (e.g. 0.10 W/cm^2), the signal-to-noise level is very small in the absence of the plasmonic enhancement effect and decreases rapidly with increasing temperature approaching the background level for T > 30 K (see Figure S8). This is because of the dominance of the nonradiative recombination processes at low carrier concentration.[66] With the plasmonic enhancement effect, the signal-to-noise ratio increases significantly at low temperatures but again it decreases to the background level for T > 65 K (Figure S8), suggesting that the carrier concentration is still not high enough to saturate the nonradiative recombination active sites that increases with increasing temperature.[59] As a result, at low excitation intensity, the PL enhancement is limited to a narrow temperature range as shown by the black line in Figure 4b. With increasing P, the enhancement factor peaks at progressively higher temperatures as the saturation of nonradiative recombination sites extends to higher temperatures with increasing carrier concentration.

The contribution of the plasmon generated and captured carriers to the QW PL can be quantified at least partially by analyzing the dependence of F on T and P. To this end, we assume that carriers created by plasmon excitation of the region close to the AuNR-GaAs interface cannot migrate to the well at 10 K, the lowest temperature that can be achieved using our cryo system. As a result, the PL enhancement at the lowest temperature is assumed to originate from the Purcell enhancement effect. The results reported by Estrin *et al*[52] indicate that the Purcell enhancement factor decreases with temperature only slowly. The fact that F increases up to certain temperature for our sample indicates that the temperature dependence of the PL

enhancement factor is dominated by the contribution of carriers captured from the capping layer, and hence the Purcell factor can reasonably be assumed constant. We note that these assumptions underestimate the contribution of the PL enhancement due to plasmon generated and captured carriers. With this in mind, the enhancement factors obtained at different P in Figure 4b can be normalized dividing by the corresponding value at 10 K to get the results plotted in Figure 4c. The normalized plots show that the contribution of captured carriers increases with increasing P as more carriers are generated inside the capping layer and the nonradiative recombination sites are saturated. We can then quantify the contribution of plasmon generated and captured carriers using a parameter ρ that is defined as follows.

$$\rho(P) = \frac{F_C(P)}{F_0(P)} \qquad (3)$$

Where F_0 is the PL enhancement factor at the lowest temperature (10 K), and F_C is the enhancement factor due to carriers generated by plasmon pumping of the capping layer and transferred to the well. F_C is determined by subtracting F_0 from the total F at the peak temperature, $F_C = F_{peak} - F_0$. As shown in Figure 4d, ρ increases from about 50% at P = 0.1 W/cm^2 to about 250% at P = 0.95 W/cm^2. Interestingly, the value slightly decreases with P further increasing due to saturation of the efficiency of carrier transfer to the well, similar to efficiency droop in light-emitting diodes.[67]

The enhancement factors for the QWs with d = 5 nm and d = 10 nm are compared in Figure 5, where F values are mapped on T-P axes using color scale. The different trends for the two QWs reflect different contribution of absorption and emission enhancements by the plasmonic coupling. For d = 5 nm, in which the Purcell factor is the dominant enhancement mechanism, F increases with the increasing P at all temperatures as shown in Figure 5a. The normalized map in Figure 5b shows that the contribution of plasmon generated and captured carriers is important

only at high incident laser power, indicating the need for high carrier density to saturate the high defect density before carriers can be captured by the well. For this barely capped QW, the contribution of captured carriers becomes negligible for $T > 40$ K (Figure 5b) as more nonradiative recombination sites are activated and the shallow capping layer does not provide efficient confinement.

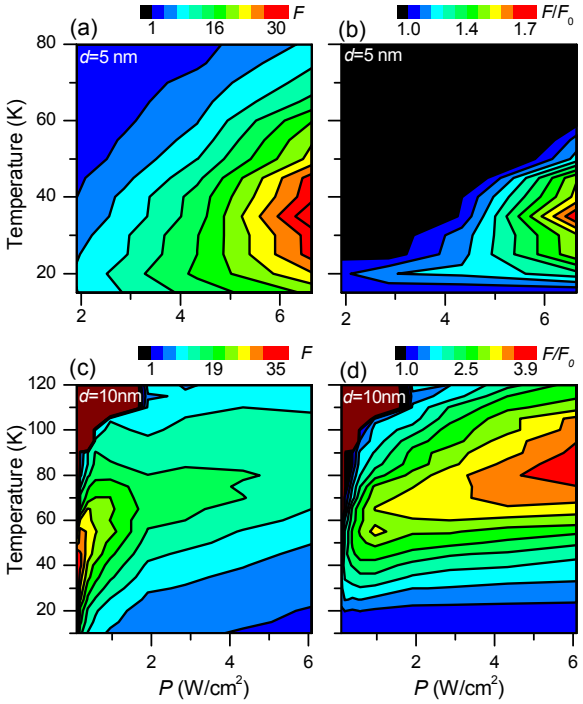

Figure 5 Two-dimensional map of the PL intensity enhancement factor F on T-P axes, representing the F values with color scale for the QW with $d = 5$ nm (a, b), and $d = 10$ nm (c, d). The color scale in (b) and (d) represent the ratio $F(P, T)/F(P, T_0)$ that indicate the contribution of plasmon generated and captured carriers to the PL enhancement. Representative line plots are provided in Figure S9.

For $d = 10$ nm, the dependence of F on P may appear complicated at first sight of the 2D map in Figure 5c because of the different enhancement mechanisms depending on temperature. For $T < 50$ K, F decreases exponentially as shown in Figure 5c (see also Figure S9c). This is because the increase in the PL intensity as a function of P without the AuNRs is faster than the intensity increase due to the plasmonic enhancement. Because at low temperature only very

small fraction of the carriers generated by the plasmon field confined at the AuNR-GaAs interface are expected to migrate and captured by the well due to the small diffusion coefficient (Figure S6). For $45 < T < 95$, F first increases as a function of P and then decreases (Figures 5c and S9c). The normalized plots indicate that the contribution of plasmon generated and captured carriers continue to be important even at relatively high temperatures with increasing P (Figures 5d and S9d). However, at sufficiently high temperature, carrier confinement becomes inefficient and the overall trend of the PL enhancement is essentially determined by the Purcell factor that is expected to increase with increasing P.

3.3 QW-plasmon coupling length. From the results discussed in Sections 3.1 and 3.2, we conclude that plasmon pumped excitation of the barrier close to the AuNR-GaAs interface appears to have the dominant contribution to the PL enhancement when d is increased from 5 nm to 10 nm. However, it is important to note that the absorption and Purcell enhancement effects are not mutually exclusive. The absorption enhancement increases the carrier concentration inside the well and the Purcell enhancement effect increases the photon extraction efficiency. The results in Figure 6 shade some light into this. The enhancement factor decreases drastically when d is increased from 10 nm to 15 nm. For the specific example shown in Figure 6, the average F has decreased from ~31 (for d = 10 nm) to ~2.5 (for d = 15 nm). The enhancement factor for d = 10 nm can be as high as ~80 depending on the AuNR distribution within the illuminated area (see Figure S10), while the maximum F value observed for d = 15 nm is ~4. As shown by the red circles in Figure 6, for d = 15 nm, F increases with increasing temperature achieving a maximum at ~73 K, compared to ~47 K for d = 10 nm. The shift in the peak temperature indicates improved carrier confinement and suppression of nonradiative losses with increasing thickness of the GaAs capping layer. It is interesting to note that the peak value of F_C

has decreased from 17.2 to 1.3 when d is increased from 10 nm to 15 nm. This corresponds to $F_{C,15nm}/F_{C,10nm}$ ratio of 0.08, which is much smaller than $1/e$ that is commonly used to define decay lengths.

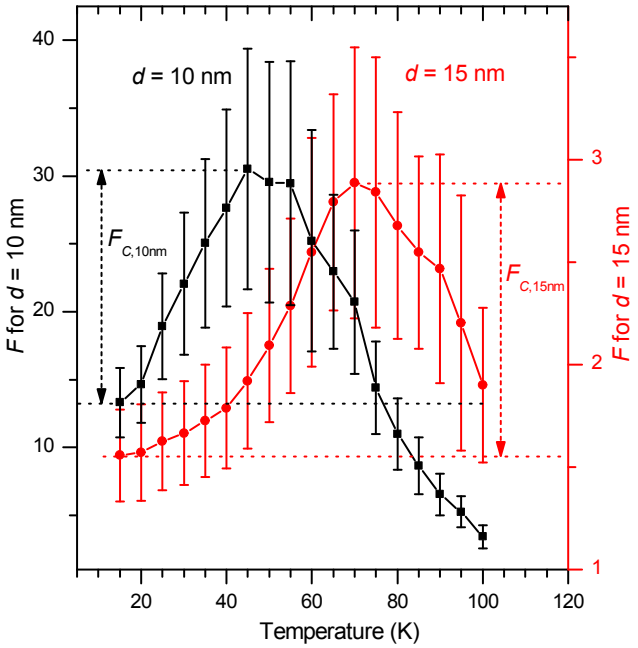

Figure 6 Temperature dependence of the PL intensity enhancement factor for InGaAs/GaAs QW with d = 10 nm (left y-axis) and d = 15 nm (right y-axis) at P = 0.14 W/cm^2. For each QW, the contribution of the plasmon generated/captured carriers to the overall PL enhancement factor is indicated by the vertical dashed line with double arrows.

This drastic decline of enhancement factor per 5 nm increase of capping layer cannot simply be attributed to short carrier diffusion length (L_d) that is related to short carrier lifetime (τ), $L_d = \sqrt{D\tau}$. It is rather characteristic of the near-field decay length. It appears that the QW-plasmon coupling at the emission wavelength is still strong at 10 nm separation and becomes negligible at 15 nm. The near-field and diffusion lengths can be extracted by repeating similar measurements on broad range of GaAs capping layer thickness as illustrated for InAs/InGaAs/GaAs quantum dot sample at room temperature.[41] Determining the carrier diffusion length provides a simple route for determining the carrier lifetime.

According to eq. (1), the emission enhancement factor F_e becomes large when the initial radiative efficiency η_r is small. As shown in Figure S11, the QW with d = 5 nm has the lowest relative quantum yield. However, the highest overall PL intensity enhancement is observed for d = 10 nm, indicating the significance of absorption enhancement. These observations suggest that the capping layer thickness can be optimized to maximize the enhancement further. In addition, the dielectric spacing between the semiconductor and the metal should be optimized such that hot electron transfer is blocked and near-field coupling is maximized.

We note that further insight into the PL enhancement mechanism can be obtained by measuring the emission lifetime as a function of temperature.[52] The plasmonic enhancement effect is expected to increase both the radiative and nonradiative decay rates.[68] As a result, the PL intensity enhancement is accompanied by lifetime reduction. By comparing the intensity enhancement and lifetime reductions for different samples, the significance of nonradiative processes may be quantified as demonstrated by Murphy and co-workers.[69]

4. CONCLUSION

In summary, plasmon enhanced absorption, carrier diffusion and capture, and plasmon enhanced photon extraction are systematically investigated by analyzing the temperature dependence of the PL properties of InGaAs/GaAs single QW coupled to colloidal AuNRs. It is shown that the contribution of the absorption and emission enhancement factors to the PL enhancement depends on the GaAs capping layer thickness d. For d smaller than the near-field decay length, the Purcell enhancement factor results in dramatic increase of the external quantum efficiency of the QW that otherwise barely emits photons. When d is reasonably increased, for example to 10 nm, such that both absorption and emission enhancements due to coupling to the plasmon modes are strong, the rates of carrier capture by the well and photon extraction out of

the well are enhanced considerably leading to up to 80 fold PL enhancement depending on temperature and distribution of the plasmonic gold nanorods. The temperature dependence of the PL enhancement factor appears to follow the temperature dependence of carrier diffusion coefficient in GaAs. Our analysis suggests that colloidal plasmonic nanoparticles can be used as simple probes for investigating carrier transport phenomena in arbitrary semiconductor heterostructures.

ASSOCIATED CONTENT

Supporting Information. The Supporting Information is available free of charge on the ACS Publications website. The following files are available.

Eleven supporting figures and descriptions (file type, i.e., PDF)

AUTHOR INFORMATION

Corresponding Author

*Terefe G. Habteyes, <habteyes@unm.edu>

Author Contributions

The manuscript was written through contributions of all authors. All authors have given approval to the final version of the manuscript.

Notes

None

ACKNOWLEDGMENT

This research has been supported by the U.S. National Science Foundation Grant No. 1651478 and the U.S. Air Force Office of Scientific Research Grant No. FA9550-18-1-0512.

References

(1) Okamoto, K.; Niki, I.; Shvartser, A.; Narukawa, Y.; Mukai, T.; Scherer, A., Surface-Plasmon-Enhanced Light Emitters Based on InGaN Quantum Wells. *Nat. Mater.* **2004,** *3*, 601-605.

(2) Lu, Y. C.; Chen, C. Y.; Yeh, D. M.; Huang, C. F.; Tang, T. Y.; Huang, J. J.; Yang, C. C., Temperature Dependence of the Surface Plasmon Coupling with an InGaN/GaN Quantum Well. *Appl. Phys. Lett.* **2007,** *90*, 193103.

(3) Yeh, D. M.; Huang, C. F.; Chen, C. Y.; Lu, Y. C.; Yang, C. C., Localized Surface Plasmon-Induced Emission Enhancement of a Green Light-Emitting Diode. *Nanotechnology* **2008,** *19*, 345201.

(4) Kwon, M. K.; Kim, J. Y.; Kim, B. H.; Park, I. K.; Cho, C. Y.; Byeon, C. C.; Park, S. J., Surface-Plasmon-Enhanced Light-Emitting Diodes. *Adv. Mater.* **2008,** *20*, 1253- 1257.

(5) Toropov, A. A.; Shubina, T. V.; Jmerik, V. N.; Ivanov, S. V.; Ogawa, Y.; Minami, F., Optically Enhanced Emission of Localized Excitons in $In_xGa_{1-x}N$ Films by Coupling to Plasmons in a Gold Nanoparticle. *Phys. Rev. Lett.* **2009,** *103*, 037403.

(6) Lu, Y. C.; Chen, Y. S.; Tsai, F. J.; Wang, J. Y.; Lin, C. H.; Chen, C. Y.; Kiang, Y. W.; Yang, C. C., Improving Emission Enhancement in Surface Plasmon Coupling with an InGaN/GaN Quantum Well by Inserting a Dielectric Layer of Low Refractive Index between Metal and Semiconductor. *Appl. Phys. Lett.* **2009,** *94*, 233113.

(7) Henson, J.; Dimakis, E.; DiMaria, J.; Li, R.; Minissale, S.; Dal Negro, L.; Moustakas, T. D.; Paiella, R., Enhanced Near-Green Light Emission from InGaN Quantum Wells by Use of Tunable Plasmonic Resonances in Silver Nanoparticle Arrays. *Opt. Express* **2010,** *18*, 21322-21329.

(8) Jang, L. W.; Jeon, D. W.; Sahoo, T.; Jo, D. S.; Ju, J. W.; Lee, S. J.; Baek, J. H.; Yang, J. K.; Song, J. H.; Polyakov, A. Y.; Lee, I. H., Localized Surface Plasmon Enhanced Quantum Efficiency of InGaN/GaN Quantum Wells by Ag/SiO_2 Nanoparticles. *Opt. Express* **2012,** *20*, 2116-2123.

(9) Dobrovolskas, D.; Mickevicius, J.; Tamulaitis, G.; Chen, H. S.; Chen, C. P.; Jung, Y. L.; Kiang, Y. W.; Yang, C. C., Spatially Resolved Study of InGaN Photoluminescence Enhancement by Single Ag Nanoparticles. *J. Phys. D-Appl. Phys.* **2013,** *46*, 145105.

(10) Li, Y.; Liu, B.; Zhang, R.; Xie, Z. L.; Zhuang, Z.; Dai, J. P.; Tao, T.; Zhi, T.; Zhang, G. G.; Chen, P.; Ren, F. F.; Zhao, H.; Zheng, Y. D., Investigation of Surface-Plasmon Coupled Red Light Emitting InGaN/GaN Multi-Quantum Well with Ag Nanostructures Coated on GaN Surface. *J. Appl. Phys.* **2015,** *117*, 153103.

(11) Iida, D.; Fadil, A.; Chen, Y. T.; Ou, Y. Y.; Kopylov, O.; Iwaya, M.; Takeuchi, T.; Kamiyama, S.; Akasaki, I.; Ou, H. Y., Internal Quantum Efficiency Enhancement of GaInN/GaN Quantum-Well Structures Using Ag Nanoparticles. *AIP Adv.* **2015,** *5*, 097169.

(12) Zhang, C.; Tang, N.; Shang, L. L.; Fu, L.; Wang, W. Y.; Xu, F. J.; Wang, X. Q.; Ge, W. K.; Shen, B., Local Surface Plasmon Enhanced Polarization and Internal Quantum Efficiency of Deep Ultraviolet Emissions from AlGaN-Based Quantum Wells. *Sci Rep* **2017,** *7*, 2358.

(13) Wu, F.; Sun, H. D.; Ajia, I. A.; Roqan, I. S.; Zhang, D. L.; Dai, J. N.; Chen, C. Q.; Feng, Z. C.; Li, X. H., Significant Internal Quantum Efficiency Enhancement of GaN/AlGaN Multiple Quantum Wells Emitting at ~350 nm via Step Quantum Well Structure Design. *J. Phys. D-Appl. Phys.* **2017,** *50*, 245101.

(14) Chang, C. C.; Sharma, Y. D.; Kim, Y. S.; Bur, J. A.; Shenoi, R. V.; Krishna, S.; Huang, D. H.; Lin, S. Y., A Surface Plasmon Enhanced Infrared Photodetector Based on InAs Quantum Dots. *Nano Lett.* **2010,** *10*, 1704-1709.

(15) Senanayake, P.; Hung, C. H.; Shapiro, J.; Lin, A.; Liang, B. L.; Williams, B. S.; Huffaker, D. L., Surface Plasmon-Enhanced Nanopillar Photodetectors. *Nano Lett.* **2011,** *11*, 5279-5283.

(16) Luo, L. B.; Xie, W. J.; Zou, Y. F.; Yu, Y. Q.; Liang, F. X.; Huang, Z. J.; Zhou, K. Y., Surface Plasmon Propelled High-Performance CdSe Nanoribbons Photodetector. *Opt. Express* **2015,** *23*, 12979-12988.

(17) Miao, J. S.; Hu, W. D.; Jing, Y. L.; Luo, W. J.; Liao, L.; Pan, A. L.; Wu, S. W.; Cheng, J. X.; Chen, X. S.; Lu, W., Surface Plasmon-Enhanced Photodetection in Few Layer MoS_2 Phototransistors with Au Nanostructure Arrays. *Small* **2015,** *11*, 2392-2398.

(18) Yu, P.; Wu, J.; Ashalley, E.; Govorov, A.; Wang, Z. M., Dual-Band Absorber for Multispectral Plasmon-Enhanced Infrared Photodetection. *J. Phys. D-Appl. Phys.* **2016,** *49*, 365101.

(19) Qi, Z. Y.; Zhai, Y. S.; Wen, L.; Wang, Q. L.; Chen, Q.; Iqbal, S.; Chen, G. D. A.; Xu, J.; Tu, Y., Au Nanoparticle-Decorated Silicon Pyramids for Plasmon-Enhanced Hot Electron Near-Infrared Photodetection. *Nanotechnology* **2017,** *28*, 275202.

(20) Oulton, R. F.; Sorger, V. J.; Zentgraf, T.; Ma, R. M.; Gladden, C.; Dai, L.; Bartal, G.; Zhang, X., Plasmon Lasers at Deep Subwavelength Scale. *Nature* **2009,** *461*, 629-632.

(21) Liu, X. F.; Zhang, Q.; Yip, J. N.; Xiong, Q. H.; Sum, T. C., Wavelength Tunable Single Nanowire Lasers Based on Surface Plasmon Polariton Enhanced Burstein-Moss Effect. *Nano Lett.* **2013,** *13*, 5336-5343.

(22) Cao, F. Z.; Niu, L. Z.; Tong, J. H.; Li, S. T.; Hayat, A.; Wang, M.; Zhai, T. R.; Zhang, X. P., Hybrid Lasing in a Plasmonic Cavity. *Opt. Express* **2018,** *26*, 13383-13389.

(23) Atwater, H. A.; Polman, A., Plasmonics for Improved Photovoltaic Devices. *Nat Mater* **2010,** *9*, 205-213.

(24) Pillai, S.; Green, M. A., Plasmonics for Photovoltaic Applications. *Solar Energy Materials and Solar Cells* **2010,** *94*, 1481-1486.

(25) Zhou, N.; Lopez-Puente, V.; Wang, Q.; Polavarapu, L.; Pastoriza-Santos, I.; Xu, Q. H., Plasmon-Enhanced Light Harvesting: Applications in Enhanced Photocatalysis, Photodynamic Therapy and Photovoltaics. *RSC Adv.* **2015,** *5*, 29076-29097.

(26) Wu, N. Q., Plasmonic Metal-Semiconductor Photocatalysts and Photoelectrochemical Cells: A Review. *Nanoscale* **2018,** *10*, 2679-2696.

(27) Zhao, H. L.; Zheng, X. Y.; Feng, X. H.; Li, Y., CO_2 Reduction by Plasmonic Au Nanoparticle-Decorated TiO_2 Photocatalyst with an Ultrathin Al_2O_3 Interlayer. *J. Phys. Chem. C* **2018,** *122*, 18949-18956.

(28) Li, Z.; Shi, L.; Franklin, D.; Koul, S.; Kushima, A.; Yang, Y., Drastic Enhancement of Photoelectrochemical Water Splitting Performance over Plasmonic Al@TiO_2 Heterostructured Nanocavity Arrays. *Nano Energy* **2018,** *51*, 400-407.

(29) Li, C. P.; Wang, P.; Li, H. J.; Wang, M. M.; Zhang, J.; Qi, G. H.; Jin, Y. D., Plasmon-Driven Water Splitting Enhancement on Plasmonic Metal-Insulator-Semiconductor Hetero-Nanostructures: Unraveling the Crucial Role of Interfacial Engineering. *Nanoscale* **2018,** *10*, 14290-14297.

(30) Enrichi, F.; Quandt, A.; Righini, G. C., Plasmonic Enhanced Solar Cells: Summary of Possible Strategies and Recent Results. *Renew. Sust. Energ. Rev.* **2018,** *82*, 2433-2439.

(31) Naik, G. V.; Welch, A. J.; Briggs, J. A.; Solomon, M. L.; Dionne, J. A., Hot-Carrier-Mediated Photon Upconversion in Metal-Decorated Quantum Wells. *Nano Lett.* **2017,** *17*, 4583-4587.

(32) Kholmicheva, N.; Romero, L. R.; Cassidy, J.; Zamkov, M., Prospects and Applications of Plasmon-Exciton Interactions in the Near-Field Regime. *Nanophotonics* **2019,** *8*, 613-628.

(33) Kinkhabwala, A.; Yu, Z. F.; Fan, S. H.; Avlasevich, Y.; Mullen, K.; Moerner, W. E., Large Single-Molecule Fluorescence Enhancements Produced by a Bowtie Nanoantenna. *Nat. Photonics* **2009,** *3*, 654-657.

(34) Itoh, T.; Yamamoto, Y. S.; Ozaki, Y., Plasmon-Enhanced Spectroscopy of Absorption and Spontaneous Emissions Explained Using Cavity Quantum Optics. *Chem. Soc. Rev.* **2017,** *46*, 3904-3921.

(35) Khurgin, J. B.; Sun, G.; Soref, R. A., Practical Limits of Absorption Enhancement Near Metal Nanoparticles. *Appl. Phys. Lett.* **2009,** *94*, 071103.

(36) Sun, G.; Khurgin, J. B.; Soref, R. A., Practical Enhancement of Photoluminescence by Metal Nanoparticles. *Appl. Phys. Lett.* **2009,** *94*, 101103.

(37) Liu, S. Y.; Huang, L.; Li, J. F.; Wang, C.; Li, Q.; Xu, H. X.; Guo, H. L.; Meng, Z. M.; Shi, Z.; Li, Z. Y., Simultaneous Excitation and Emission Enhancement of Fluorescence Assisted by Double Plasmon Modes of Gold Nanorods. *J. Phys. Chem. C* **2013,** *117*, 10636-10642.

(38) Palacios, E.; Park, S.; Lauhon, L.; Aydin, K., Identifying Excitation and Emission Rate Contributions to Plasmon-Enhanced Photoluminescence from Monolayer MoS_2 Using a Tapered Gold Nanoantenna. *ACS Photon.* **2017,** *4*, 1602-1606.

(39) Hobden, M. V.; Sturge, M. D., The Optical Absorption Edge of Gallium Arsenide. *Proc. Phys. Soc.* **1961,** *78*, 615-616.

(40) Sturge, M. D., Optical Absorption of Gallium Arsenide between 0.6 and 2.75 eV. *Phys. Rev.* **1962,** *127*, 768-773.

(41) Haq, S.; Addamane, S.; Kafle, B.; Huang, D.; Balakrishnan, G.; Habteyes, T. G., Active Mediation of Plasmon Enhanced Localized Exciton Generation, Carrier Diffusion and Enhanced Photon Emission. *Sci Rep* **2017,** *7*, 864.

(42) Tan, S. J.; Argondizzo, A.; Ren, J. D.; Liu, L. M.; Zhao, J.; Petek, H., Plasmonic Coupling at a Metal/Semiconductor Interface. *Nat. Photon.* **2017,** *11*, 806- 812.

(43) Kafle, B.; Gieri, P.; Kookhaee, H.; Tesema, T. E.; Haq, S.; Manjavacas, A.; Habteyes, T. G., Robust Charge Transfer Plasmons in Metallic Particle–Film Systems. *ACS Photon.* **2018,** *5*, 4022-4029.

(44) Habteyes, T. G., Direct Near-Field Observation of Orientation-Dependent Optical Response of Gold Nanorods. *J. Phys. Chem. C* **2014,** *118*, 9119-9127.

(45) Thomas, K. G.; Barazzouk, S.; Ipe, B. I.; Joseph, S. T. S.; Kamat, P. V., Uniaxial Plasmon Coupling through Longitudinal Self-Assembly of Gold Nanorods. *J. Phys. Chem. B* **2004,** *108*, 13066-13068.

(46) Funston, A. M.; Novo, C.; Davis, T. J.; Mulvaney, P., Plasmon Coupling of Gold Nanorods at Short Distances and in Different Geometries. *Nano Lett.* **2009,** *9*, 1651-1658.

(47) Shao, L.; Woo, K. C.; Chen, H. J.; Jin, Z.; Wang, J. F.; Lin, H. Q., Angle- and Energy-Resolved Plasmon Coupling in Gold Nanorod Dimers. *ACS Nano* **2010,** *4*, 3053-3062.

(48) Slaughter, L. S.; Wu, Y. P.; Willingham, B. A.; Nordlander, P.; Link, S., Effects of Symmetry Breaking and Conductive Contact on the Plasmon Coupling in Gold Nanorod Dimers. *ACS Nano* **2010,** *4*, 4657-4666.

(49) Abtahi, S. M. H.; Burrows, N. D.; Idesis, F. A.; Murphy, C. J.; Saleh, N. B.; Vikesland, P. J., Sulfate-Mediated End-to-End Assembly of Gold Nanorods. *Langmuir* **2017,** *33*, 1486-1495.

(50) Henson, J.; Bhattacharyya, A.; Moustakas, T. D.; Paiella, R., Controlling the Recombination Rate of Semiconductor Active Layers via Coupling to Dispersion-Engineered Surface Plasmons. *J. Opt. Soc. Am. B-Opt. Phys.* **2008,** *25*, 1328-1335.

(51) Henson, J.; Heckel, J. C.; Dimakis, E.; Abell, J.; Bhattacharyya, A.; Chumanov, G.; Moustakas, T. D.; Paiella, R., Plasmon Enhanced Light Emission from InGaN Quantum Wells via Coupling to Chemically Synthesized Silver Nanoparticles. *Appl. Phys. Lett.* **2009,** *95*, 151109.

(52) Estrin, Y.; Rich, D. H.; Keller, S.; DenBaars, S. P., Temperature Dependence of Exciton-Surface Plasmon Polariton Coupling in Ag, Au, and Al Films on $In_xGa_{1-x}N$/GaN Quantum Wells Studied with Time-Resolved Cathodoluminescence. *J. Appl. Phys.* **2015,** *117*, 043105.

(53) Joyce, M. J.; Gal, M.; Tann, J., Observation of Interface Defects in Strained InGaAs-GaAs by Photoluminescence Spectroscopy. *J. Appl. Phys.* **1989,** *65*, 1377-1379.

(54) Gourley, P. L.; Fritz, I. J.; Dawson, L. R., Controversy of Critical Layer Thickness for InGaAs/GaAs Strained-Layer Epitaxy. *Appl. Phys. Lett.* **1988,** *52*, 377-379.

(55) Shen, W. Z.; Tang, W. G.; Li, Z. Y.; Shen, X. C.; Wang, S. M.; Andersson, T., Optical Studies of Strained InGaAs/GaAs Single Quantum-Wells. *Appl. Surf. Sci.* **1994,** *78*, 315-320.

(56) Jiang, D. S.; Jung, H.; Ploog, K., Temperature-Dependence of Photoluminescence from GaAs Single and Multiple Quantum-Well Heterostructures Grown by Molecular-Beam Epitaxy. *J. Appl. Phys.* **1988,** *64*, 1371-1377.

(57) Stillman, G. E.; Wolfe, C. M.; Dimmock, J. O., Hall Coefficient Factor for Polar Mode Scattering in n-Type GaAs. *J. Phys. Chem. Solids* **1970,** *31*, 1199-1204.

(58) Blakemore, J. S., Semiconducting and Other Major Properties of Gallium-Arsenide. *J. Appl. Phys.* **1982,** *53*, R123-R181.

(59) Lambkin, J. D.; Dunstan, D. J.; Homewood, K. P.; Howard, L. K.; Emeny, M. T., Thermal Quenching of the Photoluminescence of InGaAs/GaAs and InGaAs/AlGaAs Strained-Layer Quantum-Wells. *Appl. Phys. Lett.* **1990,** *57*, 1986-1988.

(60) Gurioli, M.; Vinattieri, A.; Colocci, M.; Deparis, C.; Massies, J.; Neu, G.; Bosacchi, A.; Franchi, S., Temperature-Dependence of the Radiative and Nonradiative Recombination Time in GaAs/$Al_xGa_{1-x}As$ Quantum-Well Structures. *Phys. Rev. B* **1991,** *44*, 3115-3124.

(61) Weber, S.; Limmer, W.; Thonke, K.; Sauer, R.; Panzlaff, K.; Bacher, G.; Meier, H. P.; Roentgen, P., Thermal Carrier Emission from a Semiconductor Quantum-Well. *Phys. Rev. B* **1995,** *52*, 14739-14747.

(62) Li, J.; Ong, H. C., Temperature Dependence of Surface Plasmon Mediated Emission from Metal-Capped ZnO Films. *Appl. Phys. Lett.* **2008,** *92*, 121107.

(63) Welch, D. F.; Wicks, G. W.; Eastman, L. F., Luminescence Line-Shape Broadening Mechanisms in GaInAs/AlInAs Quantum Wells. *Appl. Phys. Lett.* **1985,** *46*, 991-993.

(64) Yoshimura, H.; Bauer, G. E. W.; Sakaki, H., Carrier-Induced Shift and Broadening of Optical-Spectra in an $Al_xGa_{1-x}As$/GaAs Quantum Well with a Gate Electrode. *Phys. Rev. B* **1988,** *38*, 10791-10797.

(65) Skolnick, M. S.; Nash, K. J.; Saker, M. K.; Bass, S. J.; Claxton, P. A.; Roberts, J. S., Free-Carrier Effects on Luminescence Linewidths in Quantum-Wells. *Appl. Phys. Lett.* **1987,** *50*, 1885-1887.

(66) Walker, A. W.; Heckelmann, S.; Karcher, C.; Hohn, O.; Went, C.; Niemeyer, M.; Bett, A. W.; Lackner, D., Nonradiative Lifetime Extraction Using Power-Dependent Relative Photoluminescence of III-V Semiconductor Double-Heterostructures. *J. Appl. Phys.* **2016,** *119*, 155702-115702.

(67) Zhao, H. P.; Liu, G. Y.; Zhang, J.; Arif, R. A.; Tansu, N., Analysis of Internal Quantum Efficiency and Current Injection Efficiency in III-Nitride Light-Emitting Diodes. *J. Disp. Technol.* **2013,** *9*, 212-225.

(68) Munechika, K.; Chen, Y.; Tillack, A. F.; Kulkarni, A. P.; Plante, I. J.-L.; Munro, A. M.; Ginger, D. S., Spectral Control of Plasmonic Emission Enhancement from Quantum Dots near Single Silver Nanoprisms. *Nano Lett.* **2010,** *10*, 2598-2603.

(69) Abadeer, N. S.; Brennan, M. R.; Wilson, W. L.; Murphy, C. J., Distance and Plasmon Wavelength Dependent Fluorescence of Molecules Bound to Silica-Coated Gold Nanorods. *ACS Nano* **2014,** *8*, 8392-8406.

Table of Content Graphic